ELSEVIER

Precambrian Research 106 (2001) 239–260

Precambrian Research

www.elsevier.com/locate/precamres

Precambrian superplumes and supercontinents: a record in black shales, carbon isotopes, and paleoclimates?

Kent C. Condie [a,*], David J. Des Marais [b], Dallas Abbott [c]

[a] *Department of Earth and Environmental Science, New Mexico Tech, Socorro, NM 87801, USA*
[b] *Ames Research Center, Moffett Field, CA 94035-1000, USA*
[c] *Lamont-Doherty Earth Observatory, Palisades, NY 10964, USA*

Received 13 January 2000; accepted 16 June 2000

Abstract

Prominent maxima in black shale abundance and in black shale/total shale ratio occur at 2.0–1.7 Ga, with less prominent peaks in the Late Neoproterozoic (800–600 Ma) and in the Late Archean (2.7–2.5 Ga). Peaks in chemical index of alteration (CIA) of shales at the same times suggest corresponding warm paleoclimates. The peaks in CIA and black shale abundance are correlated in time at a 94% confidence level. The black shale and CIA peaks may reflect the combined effects of mantle superplume events and supercontinent formation at 2.7 and 1.9 Ga. Mantle superplume events may have introduced large amounts of CO_2 into the atmosphere–ocean system, increasing depositional rates of carbon and increasing global warming. Increased black shale deposition may reflect some combination of: (1) increased oceanic hydrothermal fluxes (introducing nutrients); (2) anoxia on continental shelves; and (3) disrupted ocean currents. The apparent absence of carbon isotope anomalies at these times reflects an increase in the deposition and burial rate of both reduced and oxidized carbon. Peaks in black shale abundance at $\sim$2.1 Ga and 800–600 Ma correlate with peaks in $\delta^{13}C$ in marine carbonates, increases in atmospheric oxygen, and with high CIA values in shales. These are all consistent with higher rates of organic carbon burial in black shales at these times. These peaks may record the breakup of supercontinents at 2.2–2.0 Ga and again at 800–600 Ma, which resulted in increased numbers of partially closed marine basins, disruption of ocean currents, and increased hydrothermal vents at ocean ridges, all of which led to widespread anoxia.

Keywords: Superplume; Black Shale; Carbon Isotopes; Paleoclimates; Carbon Cycle

1. Introduction

Based on the distribution of ages of igneous rocks, Condie (1998), Isley and Abbott (1999) have suggested several superplume events in the mantle during the last 3 Ga. Supercontinent formation is associated with some of these events. To avoid confusion, we use the term superplume event as used by Isley and Abbott (1999) to refer to a relatively short-lived mantle plume event (<100 My) during which several to many large

* Corresponding author..
E-mail address: kcondie@nmt.edu (K.C. Condie).

0301-9268/01/$ - see front matter
PII: S0301-9268(00)00097-8

plumes formed and rose to the base of the lithosphere. This is similar to the usage of Larson (1991a,b), where he applied the term superplume to one or more large mantle plumes in the South Pacific during the Cretaceous. Condie (1998), furthermore, suggested that a superplume event (referred to as a plume event in the 98 paper) was part of a superevent cycle, involving also supercontinent formation and breakup. In the Condie (1998) model, the superplume event is triggered by catastrophic collapse of descending slabs through the 660 km seismic discontinuity. In another model, Greff-Lefftz and Legros (1999) suggest that resonance between the outer core and solar tidal waves at these times destablizes the D″ layer above the core, leading to the generation of numerous mantle plumes.

Larson (1991b), Kerr (1998) showed that the Mid-Cretaceous superplume event coincided with increases in surface temperature, deposition of black shales, a rise in sea level, elevated $\delta^{13}C$ in seawater, and increased production of oceanic lithosphere. To further test the idea of superplume events in the Precambrian, in this paper we compare the distribution of black shales, carbon isotopes, and paleoclimate during the Precambrian (3.0 Ga to 500 Ma) with the proposed distribution of superplume and supercontinent events.

2. Data acquisition

In compiling data to estimate abundances of black shales in the Precambrian, three problems were encountered: (1) the fact that few authors report quantitative data on the cumulative thickness of black shale in given successions; (2) a tectonic setting bias, i.e. black shales are more important in some tectonic settings than in others; and (3) the term 'black shale' has been applied to shales having a broad range of shades of gray, i.e. they contain varying amounts of organic carbon. To address the first problem, the senior author contacted via email investigators that reported Precambrian black shale in published papers as well as many investigators currently studying successions containing black shale. The following information was requested from over 300 scientists who had reported or are studying stratigraphic successions containing black shale:

1. Name, location, and age of succession (also reference to age).
2. Approximate thickness of succession.
3. Percent of shale in the succession.
4. The fraction of black + dark gray shale in the total shale.

We received $\sim 50\%$ response to the survey, and were able to use 62 of these in our compilation (Appendix A). We tried to minimize the problem of bias in tectonic setting by including only successions that appeared to have been deposited in passive margin, intracratonic, or platform basins. To further minimize the effects of different tectonic settings and also to reduce the effects of local sedimentary environment, changing sedimentary facies, and selective preservation of certain lithologies within a section, we applied the following three filters to the data: (1) only successions with > 500 m of sediment preserved were included in the compilation; (2) of the total sediments preserved in a section, $\geq 15\%$ are shales; and (3) when more than one stratigraphic section was published for a given basin or stratigraphic unit, mean thicknesses were calculated so that each basin was counted only once. Because few chemical analyses of the total carbon content of Precambrian black shales are available, all black and dark gray shales were counted as black shales in the survey. Light to medium-gray shales were not included.

The chemical index of alteration (CIA), commonly referred to as the paleoweathering index (Nesbitt and Young, 1982; Nesbitt et al., 1996), has been used to estimate the degree of chemical weathering in the source areas of shales. The CIA is calculated from the molecular proportions of oxides, where CaO is the amount in only the silicate fraction and $CIA = [Al_2O_3/(Al_2O_3 + CaO + Na_2O + K_2O)] \times 100$, molecular ratio. The higher the CIA, the greater the degree of chemical weathering in sediment sources. For example, CIA values over 85 are characteristic of residual clays in tropical climates (Nesbitt and Young, 1982). In our study we compiled chemical analyses of Precambrian shales from the tectonic settings mentioned above, and calculated average

CIA values for shales in each succession. In this compilation, we included all successions with shales, regardless of whether they contained black shales. These results, given in Appendix B, reflect the average degree of weathering of the shale sources, and thus the average paleoclimatic regime in these sources at the time of deposition.

3. Results

Our black shale results (Appendix A) include sediments ranging in age from Late Archean (= 3.0 Ga) to the end of the Neoproterozoic (0.543 Ga). A cumulative thickness histogram shows a clear maximum in black shale abundance at 2.0–1.7 Ga with smaller peaks at ~2.1 Ga and 600 Ma and the suggestion of a peak at 2.7 Ga (Fig. 1(a)). The relatively small cumulative thickness of black shales older than 2 Ga may reflect removal by erosion of older successions. Veizer (1988) suggested a half life of ~350 My for Phanerozoic platform/intracratonic successions. Correcting the black shale thickness data with this half life, the peaks at 2.0–1.7, 2.1, and 0.6 Ga are preserved, and the small peak at 2.7 Ga becomes more prominent. To minimize the effects of differing sedimentary environments and facies as well as selective erosion of shale from successions, results are also shown for the ratio of black shale to total shale with time (Fig. 1(b)). Again, peaks are apparent in the range 2.0–1.8 Ga as well as in Late Neoproterozoic (800–600 Ma) and in the Late Archean (2.7–2.5 Ga).

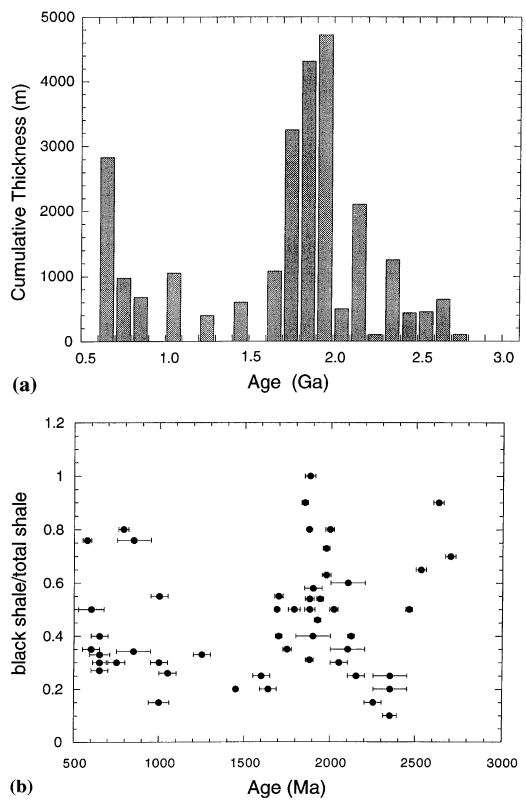

Fig. 1. Age distribution of black shale in Precambrian passive margin, cratonic, and platform successions. (a) Frequency distribution of total thickness of black shale. (b) Ratio of black shale to total shale. Error bars are one standard deviation of mean age. Data from Appendix A.

When black shales are weighted by preserved thickness, a time series (Isley and Abbott, 1999) shows three peaks in the Paleoproterozoic (i.e. ~2.0, 1.85, and 1.7 Ga), with small peaks at 600 Ma and 1.45 Ga, and a maximum near the Archean/Proterozoic boundary between 2.7 and 2.5 Ga (Fig. 2). Plotted as a time series weighted by errors in ages and by the ratio of black shale to total shale, a very strong peak occurs at 1.9 Ga, with smaller peaks at 1.7, 2.0, and 0.6 Ga, and again, three small peaks at the Archean/Proterozoic boundary (Fig. 2). Considered collectively, there is evidence of one to three well defined maxima in black shale deposition at 2.0–1.7 Ga, with a broad, less well defined maximum in the Late Neoproterozoic and one to three small maxima in the Late Archean.

Although the CIA data show considerable scatter in some sections, due perhaps to later remobilization of Ca, Na, or K, results suggest peaks in CIA at ~800–600 Ma, 1.9–1.7 Ga, and 2.9–2.7 Ga (Fig. 3). Average Phanerozoic shale, as represented by PAAS, has a CIA value of 70. From the plotted data, it would appear that the background CIA level for Precambrian shales is ~65–75. Plotted as a time series that includes errors in ages, three broad peaks are apparent in the Paleoproterozoic (at ~1.7, 1.9, and 2.1 Ga) and one or two coalescing peaks in the Late Archean (2.9–2.7 Ga) (Fig. 2). This distribution of CIA values suggests that paleoclimates were warmer

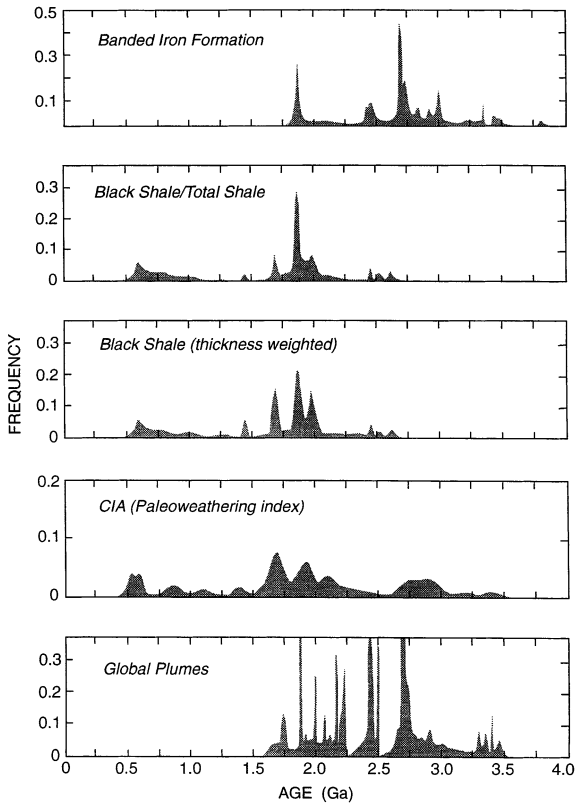

Fig. 2. Time series of black shale and CIA distributions from this study compared with BIF and global plumes from Isley and Abbott (1999). Time series generated by summing Gaussian distributions of unit area using mean ages and standard deviations from Appendices A–B.

than today in the Late Archean (2.8–2.7 Ga), Mid-Paleoproterozoic (2.0–1.7Ga), and again in the Late Neoproterozoic (at ~800–600 Ma). Despite scatter in the data, there is an overall suggestion of decreasing CIA values with time with Archean values averaging ~80, Proterozoic ~75, and Phanerozoic ~70. This trend, if real, could reflect a gradual decrease in greenhouse gases (principally CO_2) in the atmosphere with time.

3.1. Cross correlation of CIA and black shale time series

We performed a cross correlation analysis of the CIA time series with three variants of the black shale time series. The first time series has a peak height that depends only on the accuracy of the age of the black shales; the second depends on both the accuracy of the age and the total thickness of the black shales preserved at each locality; and the third depends on both the accuracy of the age and the thickness ratio of black shale to total shale in each section. The cross correlation analyses produced broadly comparable results, with best fitting time delays between CIA and the black shale time series of 29 to 1 My (Table 1). The correlation coefficients between the CIA and black shale time series ranged from 0.67 to 0.71. These coefficients are equivalent to certainties in correlation of the time series between 85 and 95% when compared to 1000 randomly generated time series with the same spectral characteristics.

Given the uncertainties in ages of both time series, the calculated time delays between the CIA time series and the black shale time series are not large. For example, the mean error of the CIA ages is 50 My, and the mean error of the black shale ages is 48 My. Therefore, calculated time lags of 29 to 1 My are effectively zero when the error in ages of the two time series are considered.

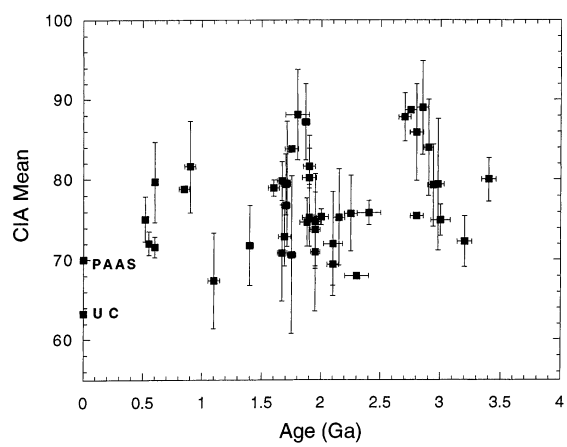

Fig. 3. Distribution of CIA in Precambrian shales from passive margin, cratonic, and platform successions. Error bars are one standard deviation of the mean values. PAAS, Proterozoic Average Australian Shale (Taylor and McLennan, 1985); UC, Average upper continental crust (Condie, 1993). CIA = $[Al_2O_3/(Al_2O_3 + CaO + Na_2O + K_2O) \times 100]$ molecular ratio, with CaO representing the silicate fraction only.

Table 1
Cross correlation analysis of black shale and CIA time series

Time series type	Time lag (My)	Correlation coefficient	Confidence level (%)
Black shale	29	0.709	94.0
Black shale weighted by thickness	1.1	0.705	94.7
Black shale weighted by thickness ratio	8.9	0.667	85.7

The correlation coefficient values of CIA with the black shale time series are not meaningful by themselves. A given correlation coefficient between two time series depends on the properties of the time series (their spectral characteristics) as well as the overall similarities between the time series. For this reason, we have calculated the correlation coefficient values between each of the black shale time series and 1000 randomly generated time series (as in Isley and Abbott, 1999). Although the overall ranges in correlation coefficient are similar (roughly between 0.3 and 0.8), each of the time series has a slightly different level of confidence for the same value of the correlation coefficient (Table 1). The highest correlation coefficient value between two time series is 0.709 between the unweighted black shales and CIA. However, the level of confidence of this cross correlation is slightly lower (94%) than that of the smaller correlation coefficent (0.704) between the black shale data weighted for thickness versus CIA. This latter correlation has a 94.7% confidence level. Both of these correlation coefficients could occur by random chance, but the probability is $<7\%$. These high confidence levels for the correlation coefficients support the idea that peaks in black shale abundance are temporally associated with increases in the CIA paleoweathering indices of black shale sequences. Therefore, the same process could have produced both high abundances of black shales and increased weathering of the sources of the shale sequences.

3.2. Superplumes, supercontinents, and the carbon cycle

Before attempting to interpret the distribution of black shales and paleoclimates in the Precambrian, it is necessary to discuss the carbon cycle and how it may respond to superplume events and to the formation and breakup of supercontinents.

The biogeochemical cycle can be envisioned as an integrated system of carbon reservoirs linked by processes. In Fig. 4, these reservoirs and processes are depicted as boxes and arrows, respectively. Carbon enters the ocean–atmosphere system by weathering, volcanism and metamorphism. Part of this carbon is in a reduced state because it includes organic carbon remobilized during destruction of older sediments. In the surface environment, carbon is rapidly cycled through the biosphere (path a, Fig. 4). The amounts of organic carbon and carbonate buried depend upon global rates of erosion and sedimentation (Derry et al., 1992) and upon recycling processes on the sea floor (Betts and Holland, 1991). If the average degree of reduction of buried carbon differs from that of the carbon entering the surface environment, then a net transfer of oxidizing or reducing power must occur between the carbon cycle and the cycles of other elements, principally sulfur, oxygen, nitrogen, iron, and manganese.

The operation of the carbon cycle can be monitored via an isotopic mass balance (Des Marais et al., 1992):

$$\delta_{in} = f_{carb}\delta_{carb} + f_{org}\delta_{org} \quad (1)$$

where δ_{in} represents the isotopic composition of carbon entering the global surface environment comprised of the atmosphere, hydrosphere and biosphere. The right side of the equation represents the weighted-average isotopic composition of carbonate ($\delta^{13}C_{carb}$) and organic ($\delta^{13}C_{org}$) carbon being buried in sediments, and f_{carb} and f_{org} are the fractions of carbon buried in each form ($f_{carb} = 1 - f_{org}$). For timescales longer than 100

Ma, $\delta_{in} = -5\%$, the average value for crustal carbon (Holser et al., 1988). Thus, where values of sedimentary δ_{carb} and δ_{org} can be measured, it is possible to determine f_{org} for ancient carbon cycles. Note, for example, that higher values of $\delta^{13}C_{carb}$ and/or $\delta^{13}C_{org}$ indicate a higher value of f_{org}.

The processes that cycle carbon can be modulated both by crustal tectonics and by mantle plume events. A summary of possible effects of superplumes and supercontinents on the carbon cycle is given in Fig. 4. Some of the feedbacks shown in the figure have been previously discussed by Worsley et al. (1986), Des Marais (1997), Kerr (1998).

3.3. Supercontinent formation

Supercontinent assembly affects the carbon cycle in multiple ways. Continental collisions are initially a net source of CO_2 due to the burial and/or thermal destruction of sedimentary organic matter and carbonates within collisional zones (paths b–c, Fig. 4) (Bickle, 1996). Continued uplift of a supercontinent accelerates erosion of sedimentary rocks and their carbon (paths d–e). Whether this carbon source changes the $\delta^{13}C$ of seawater depends upon the ratio of the reduced carbon ($\delta^{13}C = -20 - -40$ per million) to the oxidized carbon ($\delta^{13}C = 0$ per million) that is recycled back into the oceans (path f). For example, if both carbonate and organic carbon are recycled in approximately the same ratio as their ratio prior to supercontinent formation, the $\delta^{13}C$ of seawater will not change (Des Marais et al., 1992). As the surface area of the growing supercontinent increases, weathering of surface rocks withdraws more CO_2 from the atmosphere transferring it to the continents (path g), where it is eventually returned to the oceans by erosion (path h). Increased erosion also releases more nutrients (e.g. phosphorus), increasing biological

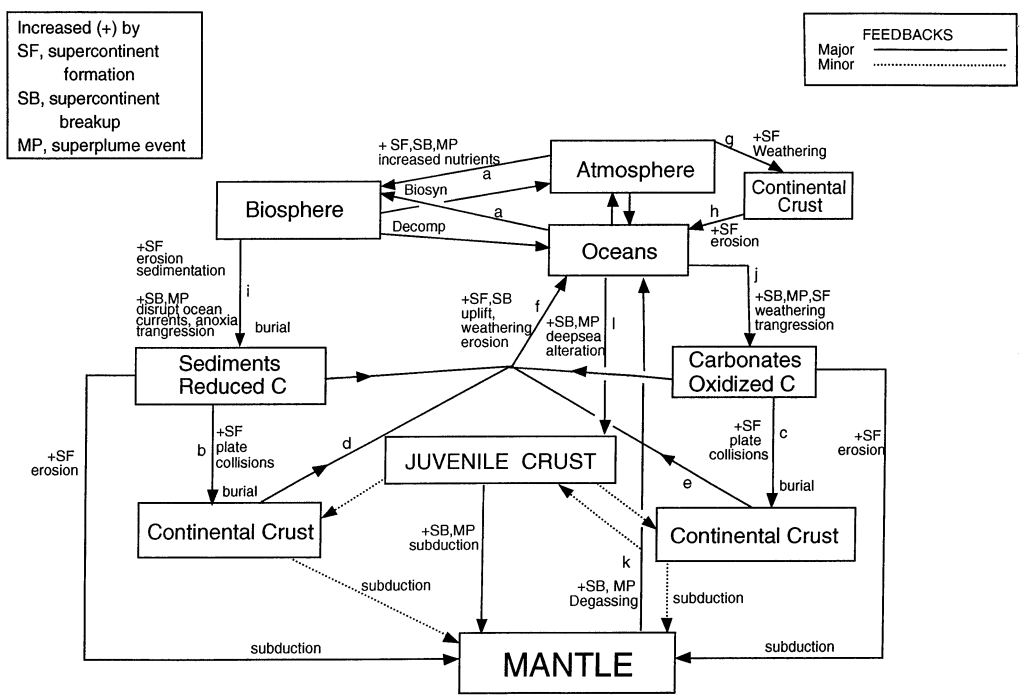

Fig. 4. Carbon reservoirs in the Earth showing possible effects of supercontinents and superplumes. Each box represents a carbon reservoir. Juvenile crust, oceanic crust + oceanic plateaus + island arcs; Biosyn, biosynthesis; Decomp, decomposition. Numbered paths refer to text discussions.

productivity (paths h, a) (Worsley and Nance, 1989). The nutrient source and CO_2 sinks can draw down atmospheric CO_2 levels, favoring cooler climates that intensify ocean circulation and thus, increase nutrient upwelling and marine productivity (Berry and Wilde, 1978). The above factors collectively promote increased burial rates of organic carbon burial, relative to carbonates, and thus can raise the $\delta^{13}C$ value of seawater. Intense drawdown of CO_2 together with increasing albedo caused by the increasing land/ocean ratio can lead to widespread glaciation.

If gas hydrates (methane–H_2O solids in shallow marine sediments) were important during the Precambrian, supercontinent formation could lead to gas hydrate evaporation as sea level drops, which would introduce biogenic carbon (as CO_2) into the atmosphere, increasing both organic and carbonate burial rates as well as increasing greenhouse warming (Haaq, 1998). Because gas hydrates contain carbon with very negative $\delta^{13}C$ values (averaging ~ -60 per million), they may offset any increase in the $\delta^{13}C$ due to extensive organic carbon burial.

As sea level falls during supercontinent formation, the ensuing regression restricts the deposition of shelf carbonates and mature clastic sediments, and the emerging shelves can accommodate deposition of extensive evaporites. Organic carbon sedimentation occurs either farther offshore or in freshwater depocenters within the interior of the supercontinent (Berner, 1983). Overall, supercontinent formation promotes higher rates of erosion and sedimentation (path i, Fig. 4) which correlate with organic carbon burial rates, and platform carbonate deposition becomes more restricted. The net result is that periods of supercontinent formation favor relatively high ratios of organic versus carbonate sedimentation and burial. If this is the case, positive carbon isotope anomalies should develop in seawater during supercontinent formation, if other processes do not obscure this effect.

3.4. Supercontinent breakup

Supercontinent breakup creates new, narrow ocean basins having restricted circulation and hydrothermally active spreading centers. These features promote anoxia in the deep ocean (path i, Fig. 4). The actively eroding escarpments along the new rift margins contribute sediments to these basins, and marine transgressions increase the rate of burial of organic and carbonate carbon on stable continental shelves. The amount of shallow marine carbonate deposition (path j), however, critically depends on redox stratification of the oceans, as reducing environments are not conducive to carbonate precipitation. Should anoxic deep-ocean water invade the shelves, it would facilitate organic carbon burial on the shelves, including the deposition of black shale.

The increase in the length of the ocean ridge network that accompanies supercontinent fragmentation promotes increased degassing of the mantle, including CO_2 (path k). Increasing atmospheric CO_2 levels and rising sea level promote warmer climates that increase weathering rates (path g) (Berner and Berner, 1997) as well as the potential for the marine water column to become stratified and for deep water to become anoxic (path i) (Berry and Wilde, 1978). Increasing carbonate in the oceans together with a growing ocean ridge system would also enhance rates of removal of seawater carbonate by deep-sea alteration (path l). To the extent that these developments enhance the fraction of carbon buried as organic matter, they would also lead to an increase in the $\delta^{13}C$ of seawater because ^{12}C is preferentially incorporated into organic carbon (Des Marais et al., 1992; Karhu and Holland, 1996; Melezhik and Fallick, 1996).

3.5. A superplume event

During a superplume event, ascending plumes warm the upper mantle and lithosphere, and thereby elevate the seafloor by thermal expansion and create oceanic plateaus by the eruption of large volumes of submarine basalt. Rising sea level triggers marine transgressions (Larson, 1991b) (path i, Fig. 4). Oceanic plateaus can locally restrict ocean currents (Kerr, 1998), thus promoting local stratification of the marine water column leading to anoxia (path i). Plume volcanism and associated extensive hydrothermal activ-

ity exhale both CO_2 and reduced constituents into the atmosphere–ocean system (Larson, 1991b; Caldeira and Rampino, 1991; Kerr, 1998). The increased CO_2 flux warms the climate and enhances weathering rates (path g) (Berner and Berner, 1997). Biological productivity is enhanced by several factors, such as increased concentrations of CO_2, increased nutrient fluxes from both hydrothermal activity (such as P, H_2, sulfides, trace metals, etc.) and enhanced weathering, and elevated temperatures due to CO_2-driven greenhouse warming (paths a). Carbonate precipitation is enhanced by the increased weathering of cations and by marine transgressions (path j). Increased hydrothermal activity on the sea floor during a superplume event would also increase the rate of deep-sea alteration, which in turn should increase the removal rate of carbonate from seawater (path l). Liberation of large amounts of SO_2 into the oceans by increased seafloor vents might decrease ocean pH, the net effect of which would be to dissolve some marine carbonate, particularly adjacent to high-temperature emanations (Kerr, 1998). However, a more acid ocean would dissolve more cations increasing the oceanic pH again. If the oceans are relatively reducing, hydrothermal exhalation of Fe^{2+} promotes siderite deposition, for example, adjacent to banded iron formations (Beukes et al., 1990). This, in turn, promotes carbonate deposition overall, because siderite is less soluble than calcite and dolomite. Organic matter burial is enhanced by increased productivity, marine transgressions and the expansion of anoxic waters, in particular onto the continental shelves (path i) (Larson, 1991b; Kerr, 1998). In summary, phenomena associated with superplumes promote the formation and deposition of both organic and carbonate carbon. It has been proposed that the relative deposition of carbonates and organic carbon reflect redox buffering of the crustal and surface environment by the redox state of the upper mantle (Holland, 1984). Redox buffering by the mantle should be even stronger during superplume events.

Subduction of carbon might play a role in determining the response of the carbon cycle to superplume events. During most of Earth history, the relative rates of subduction of carbonate and reduced carbon reflect their relative crustal abundances. If they did not, then the mean $\delta^{13}C$ values of crustal versus mantle carbon reservoirs would differ substantially today, because the preferential subduction of either oxidized or reduced carbon would have made the crust–mantle exchange of carbon an isotopically-selective process. However, the $\delta^{13}C$ values of the total crust and mantle carbon reservoirs are identical within the uncertainties of the measurements (Holser et al., 1988; Des Marais and Moore, 1984). Therefore, subduction has not favored either carbonates or organic carbon. It has been proposed that during plume events inorganic carbon is subducted and recycled faster than organic carbon (Jyotiranjan et al., 1999). If so, then the preferential retention of ^{13}C-depleted organic carbon in the surface environment would decrease the $\delta^{13}C$ value of marine carbonates deposited during superplume events. This hypothesis is eminently testable.

4. Discussion

Below we discuss three categories of events that may affect the carbon cycle. First are events that are most demonstrably superplume events at 2.7 and 1.9 Ga. The next section discusses supercontinent breakup events, and the final section discusses events that are probably not superplume events.

4.1. 2.7 and 1.9 Ga events

Based on the distribution of plume-generated mafic igneous rocks, Isley and Abbott (1999) propose two superplume events in the Late Archean at $\sim$2.5 and 2.7 Ga. Whether there are one or two such events in the Late Archean is not yet clear. If the production of significant volumes of juvenile crust is a necessary consequence of a superplume event, as suggested by Condie (1998), the 2.5-Ga event probably does not qualify because the volume of known juvenile crust of this age is only slightly above background level of continental crust formation (Fig. 1, Condie, 1998). Rather, the 2.5-Ga event is probably a subsidiary event associated with the 2.7 Ga super-

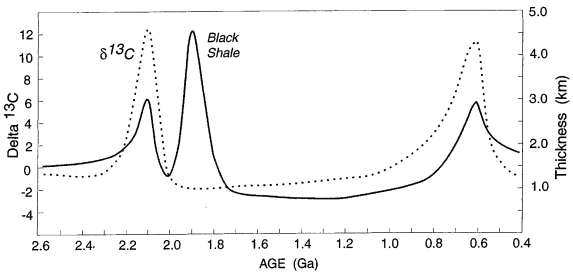

Fig. 5. Variation in $\delta^{13}C$ in marine carbonates in the Proterozoic compared to the abundance of black shales. $\delta^{13}C$ trend after Karhu and Holland (1996), Kaufman (1997).

plume event, during which large volumes of juvenile continental crust formed.

There is a good correlation between the superplume events proposed by Condie (1998) and Isley and Abbott (1999) at 2.7 and 1.9 Ga and peaks in the abundance of black shale and the warm climates implied by the CIA distribution (Fig. 3). Both of these peaks were earlier recognized from the isotopic composition of buried Precambrian kerogen (Des Marais et al., 1992). The double peak in black shale abundance at 1.9 and 1.7 Ga on the time series graph (Fig. 2) may or may not be real, and could reflect inadequate samples from the time interval between the peaks. The net effects of superplumes and supercontinent formation at 2.7 and 1.9 Ga may have introduced significant volumes of CO_2 into the atmosphere–ocean system increasing depositional rates of both organic and carbonate carbon, and increasing global warming, thus accounting for the black shale and CIA maxima at these times. A positive carbon isotope excursion is not observed in marine carbonates at 2.7 and 1.9 Ga, and therefore the relative burial rates of both reduced and oxidized carbon changed very little at 2.7 and 1.9 Ga, even as their absolute rates increased (Fig. 5). The absence of carbon isotope anomalies at these times also means that burial of plume-related carbon masked supercontinent-related carbon burial, the latter of which should favor burial of organic carbon as previously discussed. It is worth emphasizing that the absence of a negative $\delta^{13}C$ excursion in carbonates during the superplume events indicates that mantle plumes do not preferentially recycle inorganic carbon relative to reduced carbon.

If both organic and carbonate carbon were buried during the 2.7 and 1.9 Ga superplume events in approximately the same ratio at which they were buried during most of Earth history, then there should also be peaks in carbonate abundance during superplume events. Although a survey of the abundance of marine carbonates in the Precambrian record shows that they are relatively abundant in the Paleoproterozoic (an observation also made by Grotzinger and Kasting (1993), there is only a suggestion of a peak in abundances at 1.9–1.8 Ga and no evidence at 2.7 Ga (Appendix A, Fig. 6). A possible reason for the absence of strong peaks at 1.9 and 2.7 Ga may be that carbonates weather more rapidly than siliceous sediments and have not survived (Berner and Berner, 1997). This, however, requires selectively high rates of carbonate weathering at 1.9 and 2.7 Ga compared to other times in Proterozoic. Possibly many carbonates of these ages were deposited in deep ocean basins and later subducted. Widespread hydrothermal systems on the seafloor associated with plume magmatism may have produced anoxia in shallow shelf environments where carbonates are normally deposited. It is noteworthy

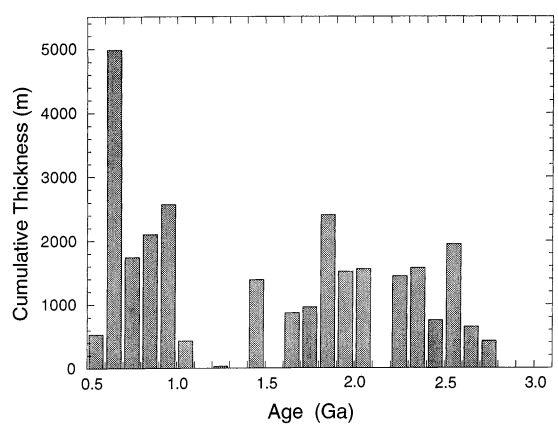

Fig. 6. Age distribution of shallow marine carbonates in Precambrian passive margin, cratonic, and platform basins. Data from Appendix A.

that the number of occurrences of marine stromatolites show peaks at 1.9 and 2.7 Ga (Hofmann, 1998), perhaps recording enhanced input of CO_2 into seawater from plume volcanism at these times. Still another potentially important sink of carbonate at 1.9 and 2.7 Ga is deep-sea alteration associated with hydrothermal springs, which would be more frequent on the sea floor due to enhanced mantle plume activity. Most of the altered oceanic crust would be subducted and returned to the mantle. A possible test for this idea is to see if 1.9 and 2.7 Ga marine greenstones have more carbonate alteration than those of other ages.

Isley and Abbott (1999) have also shown that peaks in banded iron formation (BIF) abundance correlate with the 2.7 and 1.9 Ga superplume events, with the source of the iron being primarily hydrothermal vents associated with plume magmatism. It is interesting that the decline in deposition of both black shales and BIF and a drop in paleosurface temperature (from declining CIA values) occur just after 1.7 Ga (Figs. 1–3) suggesting a similar cause for these changes. Perhaps the waning of plume magmatism and seafloor hydrothermal activity led to a decline in oceanic anoxia as both deep and shallow parts of the ocean became more oxidizing. Together with a decrease in Fe input from hydrothermal activity (needed for BIF), loss of suitable environments could lead to a decrease in black shale deposition and to an end of BIF deposition. This is supported by the first major occurrence of marine sulfates just after 1.7 Ga (Grotzinger and Kasting, 1993), suggesting increasing oxygenation of the oceans at this time. Also, the range of sulfide $\delta^{34}S$ expands ($< -20- > +20$) after 2.2 Ga, consistent with increasing seawater sulfate levels (Canfield, 1998). Decreasing amounts of CO_2 pumped into the atmosphere by plume magmas, negative feedback of continental weathering, and increasing albedo caused by the newly formed Late Archean supercontinent appear to have decreased atmospheric CO_2 levels sufficiently to cool worldwide climates after each of the superplume events. For the 2.7-Ga event, this led to widespread glaciation at 2.4–2.3 Ga (Young, 1991).

4.2. 2.0 and 0.6 Ga events

Although peaks in black shale abundance occur at about 2.0 Ga and 600 Ma (Figs. 1, 2 and 5), neither of these times has been recognized as a superplume event (Condie, 1998; Isley and Abbott, 1999). Both of these peaks, however, correlate with breakup of supercontinents, the Late Archean supercontinent at 2.2–2.0 Ga and Rodinia at 800–600 Ma (Condie, 1998). Is it possible that the increased burial of organic carbon in black shales at these times could be the result of supercontinent breakup? As previously discussed, supercontinent breakup might favor the burial of organic carbon compared to carbonate carbon (Fig. 4), and thus could result in increases in the depositional rate of black shale. Particularly important may have been the formation of numerous partially closed basins leading to widespread anoxic environments (Kerr, 1998). Supporting the supercontinent breakup model is the fact that both of these times record positive $\delta^{13}C$ anomalies in carbonates (Fig. 5), which reflect enhanced burial rates of carbon (Karhu and Holland, 1996; Des Marais, 1997; Kaufman, 1997). Also consistent with increased burial rates of organic carbon at ~ 2 Ga are paleosol data, which indicate that the oxygen level of the atmosphere rose rapidly at this time (Karhu and Holland, 1996). The appearance of multicellular organisms in the Late Neoproterozoic again suggests increasing oxygen levels in the atmosphere (Knoll and Canfield, 1998). Hence, both the 2.0 and 0.6 Ga black shale peaks may also correlate with increasing diversification of oxygen-dependent biota in response to oxygen liberated into the atmosphere–ocean system.

Why is there no evidence of growth in atmospheric oxygen at 1.9 Ga, when even greater amounts of organic carbon appear to have been buried? Possible factors contributing to minimal atmospheric oxygen input at this time include the following: (1) An increase in total surface area exposed to weathering as the Paleoproterozoic supercontinent grew may have resulted in enhanced removal of oxygen in weathering products (including oxidation of recycled organic carbon). (2) Oxidation of reduced volcanic gases emitted

by widespread submarine hydrothermal vents associated with the superplume event could also consume free oxygen in the oceans. (3) And finally, because geologic indicators of atmospheric oxygen level are not very sensitive to increases once ~10% PAL oxygen levels are reached, increases in oxygen level at 1.9 Ga may not be recognized in the geologic record.

There is a broad peak in CIA at 800–600 Ma (Figs. 2 and 3) suggesting widespread warm climates at this time. Perhaps increased ocean ridge volcanism resulting from growth of the worldwide ocean ridge system as Rodinia broke up resulted in significant CO_2 input into the atmosphere–ocean system, which in turn caused greenhouse warming leading to an overall increase in the intensity of rock weathering. Marine transgressions during breakup of this supercontinent also may have contributed to global warming.

If the 2.0 and 0.6 Ga black shale peaks correlate with supercontinent fragmentation, why is there no peak in black shale abundance at 1.5–1.4 Ga when the Paleoproterozoic supercontinent allegedly broke up (Condie, 1998)? Although there may be a small peak in black shale abundance at this time (Fig. 2), it is defined entirely by black shale from one basin, the Belt Basin in western Laurentia. Possibly other basins of this age exist that have not been accurately dated, which would reinforce this peak. Alternatively, the Paleoproterozoic supercontinent may have only partially fragmented. Supporting this idea is increasing evidence that two of the largest pieces of the Mesoproterozoic supercontinent Rodinia remained intact because they formed as part of the Late Archean supercontinent (Rogers, 1996).

4.3. 25 and 1.0 Ga events?

Based on the distribution of U/Pb zircon ages and juvenile crust, Condie (1998) suggested that a superplume event occurred at ~1.2 Ga, and Isley and Abbott (1999) suggested still another event at ~2.25 Ga from the age distribution of plume-related igneous rocks. Nowhere in the black shale, CIA, or BIF distributions is there any reflection of events at 2.25 Ga or 1.2–1.0 Ga. Again, if enhanced rates of juvenile crust formation are a necessary part of superplume events as suggested by Condie (1998), we need to re-evaluate the evidence for juvenile crust formation at these times. Recent Nd isotopic data and zircon ages important in recognizing Grenvillian juvenile crust (1.2–1.0 Ga) suggest that the estimates for the abundance of juvenile crust of this age made by Condie (1998) are high, and that a peak in juvenile crust production at this time is at least questionable and probably nonexistent (Condie, 2000). It is possible that large portions of the Late Archean supercontinent remained intact until they were incorporated in the Late Mesoproterozoic supercontinent Rodinia and that the volume of juvenile Grenvillian crust may be much smaller than originally estimated. Hence, the absence of black shale and CIA peaks at 1.2–1.0 Ga is not surprising.

The 2.25-Ga superplume event suggested by Isley and Abbott (1999) based on ages of plume-related magmas (chiefly dykes) also may not be real if juvenile crust is necessary for such an event. Very little juvenile continental crust of this age has been recognized, and in fact, this age falls in the only surviving 'age gap' in the geologic record (2.4–2.2 Ga) where significant juvenile crust has not been identified. Perhaps mantle plume activity at 2.25 Ga was localized and did not result in widespread changes in the carbon cycle, an idea consistent with the absence of black shale and CIA peaks at this time.

5. Conclusions

The results of this study suggest that superplume events in Earth history may have played an important role in influencing the carbon cycle on timescales of ≥50 My. Our data indicate the existence of maxima in black shale abundance, black shale/total shale ratio, and CIA (Chemical Index of Alteration) in shales from cratonic, passive margin, and platform sediments at 2.0–1.7 Ga, 800–600 Ma, and 2.7–2.5 Ga. At 2.7 and 1.9 Ga, the black shale and CIA peaks may reflect the combined effects of mantle superplume events and supercontinent formation, the former of which introduced massive amounts of CO_2 into the at-

mosphere–ocean system increasing depositional rates of carbon and increasing global warming. Increased black shale deposition at these times is due to some combination of: (1) increased oceanic hydrothermal fluxes (introducing nutrients); (2) anoxia driven onto continental shelves; and (3) disrupted ocean currents. The absence of carbon isotope anomalies in seawater at these times reflects an increase in the deposition and burial rates of both reduced and oxidized carbon. Peaks in black shale abundance at ~ 2.1 Ga and 800–600 Ma correlate with peaks in $?^{13}C$ in marine carbonates, increasing atmospheric oxygen, and with high shale CIA values, all of which are consistent with higher rates of organic carbon burial at these times. These peaks may record the breakup of supercontinents at 2.2–2.0 Ga and again at 800–600 Ma, which resulted in increased numbers of partially closed marine basins, disruption of ocean currents, and increased ocean ridge activity, collectively leading to widespread anoxia.

Acknowledgements

The authors are greatly appreciative of all the investigators that responded to our questionnaire on black shales, the results of which made this study possible. We also acknowledge the Exobiology Program at NASA. This is Lamont-Doherty Earth Observatory Contribution Number 6075.

Appendix A. Summary of abundances of black shales and carbonates in Precambrian successions

Geologic unit	Reference	Age (Ma)	Section thickness (m)	Black shale (m)	Shale Ratio (Black/Total)	Shale (%)	Carbonate (m)
Ramah Group Labrador	Hayashi et al. (1997)	1900 ± 50	1700	394	0.58	40	193
Neoproterozoic Central Spain Mid and Upper Series	Ugidos et al. (1997)	600 ± 20	1500	813	0.76	71	210
Bleida-Tachdamt Morocco	Leblan and Moussine-Pouchkine (1994)	790 ± 50	2500	500	0.80	25	150
Campbelland Subgroup Ghaap Group Prieska, South Africa	Altermann and Siegfried (1997); W. Altermann, 1997	2530 ± 20	3000	449	0.65	23	1950
Schmidtsdrif Subgroup Ghaap Group Prieska, South Africa	Altermann and Siegfried (1997); W. Altermann, 1997	2630 ± 20	1600	648	0.90	45	640
San Ignacio Subgroup Bolivia	Litherland et. al. (1986)	1250 ± 50	3000	396	0.33	40	30
Willyama Supergroup Broken Hill, Australia	Willis et al. (1983)	1690 ± 10	4000	600	0.50	30	200
Otavi Group	Hoffman et al. (1998)	760 ± 5	2400	0			646

Geologic unit	Reference	Age (Ma)	Section thickness (m)	Black shale (m)	Shale Ratio (Black/Total)	Shale (%)	Carbonate (m)
Namibia							
Silverton Formation South Africa	Eriksson (1994; 1998)	2150 ± 50	1200	255	0.25	85	0
Transvaal Supergroup South Africa	Eriksson (1994; 1998)	2220 ± 50	4000	0			1116
Chaibasa Formation E India	Bose et al. (1997); Rajat Mazumber, 1998	2350 ± 50	5000	350	0.10	70	0
Lower Vindhyan Supergp Central India	Bose et al. (1997); Rajat Mazumber, 1998	1050 ± 50	4000	260	0.26	25	430
Upper Vindhyan Supergp Central India	Bose et al. (1997); Rajat Mazumber, 1998; Kale and Phansalkar (1991)	1000 ± 50	3000	158	0.15	35	200
Chuar Group, Arizona	Carol Dehler, 1998	750 ± 50	2000	480	0.30	80	329
Roraima Group Guiana	Gibbs and Barron (1993)	1600 ± 50	2000	75	0.25	15	0
Sukhopit Group Yenisey Ridge, Siberia	V. A. Vernikovsky, 1998	700-550	4500	720	0.40	40	0
Tungusic Group Yenisey Ridge, Siberia	V. A. Vernikovsky, 1998	650 ± 35	5500	165	0.10	30	0
Zhdanov Group Taimyr, Siberia	V. A. Vernikovsky, 1998	650 ± 40	1000	120	0.30	40	0
Kharitonov Group Taimyr, Siberia	V. A. Vernikovsky, 1998	650 ± 40	2500	165	0.33	20	0
Malokaroi Group N Tien Shan	Andrei Khudoley, 1998	600 ± 50	1200	126	0.35	30	0
Shaler Supergroup NW Territories, Canada	Young (1981); Rainbird et al. (1996)	1000 ± 70	3600	554	0.55	28	1920
Hamersley Supergroup	Barley et al. (1997)	2460 ± 10	3000	435	0.50	29	750

Geologic unit	Reference	Age (Ma)	Section thickness (m)	Black shale (m)	Shale Ratio (Black/Total)	Shale (%)	Carbonate (m)
Western Australia	Mark Barley, 1998						
Andree Land Group East Greenland	Kasper Frederiksen, 1997	650 ± 45	1250	51	0.27	15	0
Wyloo Group Western Australia	B. Krapez, 1998 Krapez (1999)	2000 ± 30	4300	495	0.50	23	374
Mininer Group Western Australia	B. Krapez, 1998 Krapez (1999)	1925 ± 25	3700	306	0.46	18	500
Wandarry Group Western Australia	B. Krapez, 1998 Krapez (1999)	1880 ± 20	3700	1079	0.54	54	625
Cane River-Pingandy Gp Western Australia	B. Krapez, 1998 Krapez (1999)	1790 ± 20	4000	500	0.50	25	0
Mt Blair-Mt Minnie Gp Western Australia	B. Krapez, 1998 Krapez (1999)	1750 ± 30	1850	201	0.35	31	158
Bresnahan Group Western Australia	B. Krapez, 1998 Krapez (1999)	1700 ± 20	4000	1008	0.40	63	0
Neds Creek Group Western Australia	B. Krapez, 1998 Krapez and Martin (1999)	1995 ± 25	5300	1993	0.80	47	0
Horseshoe Group Western Australia	B. Krapez, 1998 Krapez and Martin (1999)	1975 ± 20	1050	628	0.63	95	210
Padbury Group Western Australia	B. Krapez, 1998 Krapez and Martin (1999)	1930 ± 20	4200	544	0.54	24	0
Robinson Range Group Western Australia	B. Krapez, 1998 Krapez and Martin (1999)	1880 ± 20	2500	248	0.31	32	0
Earaheedy Group Western Australia	B. Krapez, 1998 Krapez and Martin (1999)	1700 ± 22	8000	1540	0.55	35	667
Roan/Mwashia Groups Zambia	Richard Hanson, 1998	1000	1800	81	0.30	15	450
Changcheng Series Jixian, Hebei, China	Gao Shan, 1998	850 ± 120	4270	519	0.76	16	0
Qingbaikou Series Huailei, Hebei, China	Gao Shan, 1998	850 ± 110	760	161	0.34	62	0
Woodburn Lake Group	Eva Zaleski, 1998	2700	1000	105	0.70	15	10

Geologic unit	Reference	Age (Ma)	Section thickness (m)	Black shale (m)	Shale Ratio (Black/Total)	Shale (%)	Carbonate (m)
Canada (Baffin Isl)							
Biscay Formation	David Blake, 1998	1875 ± 5	1000	160	0.80	20	333
Kimberley, W. Australia							
Onega basin	A. Slabunov, 1998	1975 ± 10	2740	600	0.73	30	50
Kolar-Karelia	Puchtel et al. (1998)						
Whitewater Group	Chris Fedo, 1998	1850 ± 20	3000	540	0.90	20	0
Ontario, Canada							
Namoona Group	Stewart Needham, 1998	2100 ± 120	3800	665	0.35	50	950
Northern Australia							
Mt Partridge Group	Stewart Needham, 1998	2100 ± 120	2200	370	0.60	28	396
Northern Australia							
South Alligator Group	Stewart Needham, 1998	1900 ± 100	1250	250	0.40	50	175
Northern Australia							
Pocatello Formation and Brigham Group, Idaho	Paul Link, 1998	600 ± 100	4500	675	0.50	30	320
Thomson Formation	Dick Ojakangas, 1998	1878 ± 20	7500	2025	1.00	27	250
Minnesota							
Rove Formation	Dick Ojakangas, 1998	1880 ± 20	3200	800	0.50	50	250
Minnesota							
Belt Supergroup	Winston (1990)	1450 ± 10	7500	600	0.20	40	1390
Montana							
Lomagundi Group	Master (1991)	2100 ± 60	1200	120	0.40	25	213
Zimbabwe							
Piriwiri Group	Master (1991)	2000 ± 40	2100	158	0.30	25	54
Zimbabwe							
Roper Group	Donnelly and Crick (1988)	1640 ± 50	3500	406	0.20	58	0
Northern Australia	Jackson and Raiswell (1991)						
Huronian Supergroup	Bennett et al. (1991)	2350 ± 100	11000	330	0.20	15	385
Southern Canada							
Snowy Pass Supergroup	Karlstrom et al. (1983)	2350 ± 100	10000	575	0.25	23	1190
SE Wyoming							
Pahrump Group	Roberts (1974)	1000 ± 100	2250	0			327
California							
Belcher Group	Ricketts and Donaldson (1981)	2100 ± 100	8000	0			903

Geologic unit	Reference	Age (Ma)	Section thickness (m)	Black shale (m)	Shale Ratio (Black/Total)	Shale (%)	Carbonate (m)
Canada							
Coronation Supergp Canada	Galbrielse and Yorath (1992)	1950 ± 10	11400	0			524
Mt Isa Suprgroup Australia	Blake and Stewart (1992)	1750 ± 30	12000+	0			800
Windermere Supergroup Canada	Eisbacher (1985) Galbrielse and Yorath (1992)	775 ± 20	3250	0			304
McKenzie Mtns Supergp Canada	Galbrielse and Yorath (1992)	800 ± 50	7500	0			2100
Neoproterozoic Baffin Island, Canada	Jackson et al. (1978)	700 ± 50	3700	0			1110
Badaybo Siberia, Russia	Andrei K. Khudoley (1997)	650 ± 50	7800	0			3575
Uchur-Maya Siberia, Russia	Andrei K. Khudoley (1997)	650 ± 50	8200	0			3810
Fortescue Supergp Australia	Arndt et al. (1991)	2750 ± 20		0			425
	% Shale = percent shale in the section						

Appendix B. Summary of CIA values in Precambrian shales

Geologic unit	Reference	Age (Ma)	Number of samples	CIA (Mean)	CIA (std dev)
Ramah Group (Roswell Harbour Fm) Labrador	Hayashi et al. (1997)	1900 ± 50	23	66.5	6.5
Neoproterozoic, Spain	Ugidos et al. (1997)	600 ± 20			
Lower Series			8	71.6	1.3
Upper Series			10	72.1	1.5

Geologic unit	Reference	Age (Ma)	Number of samples	CIA (Mean)	CIA (std dev)
Buhwa Zimbabwe	Fedo et al. (1996)	3000 ± 100	9	75.0	2.0
Booysens Group South Africa	Wronkiewicz and Condie (1987)	2800 ± 20	23	85.9	6.1
Moodies Group South Africa	K. C. Condie, 1999	3200 ± 20	11	72.3	3.2
Mozaan Group South Africa	Wronkiewicz and Condie (1989)	2980 ± 50	49	79.4	8.2
Nzuse Group South Africa	Wronkiewicz and Condie (1989)	2940 ± 30	51	79.3	5.1
Timeball Hill Formation South Africa	Wronkiewicz and Condie (1990)	2250 ± 50	36	75.8	4.7
Silverton Formation South Africa	Wronkiewicz and Condie (1990)	2150 ± 50	23	75.3	6.0
Roodepoort Group South Africa	Wronkiewicz and Condie (1987)	2220 ± 50	30	84.0	5.8
K8 Group, Witwatersrand Supergroup, S Africa	Wronkiewicz and Condie (1987)	2850 ± 50	23	89.0	5.9
Kaladgi Group Central India	Rao et al. (1999)	1800 ± 150	10	88.1	5.7
Koolpin North Australia	Matthai and Henley (1996)	1900 ± 50	16	75.3	3.6
Roraima Group Guiana	Gibbs et al. (1986)	1600 ± 50	5	78.9	1.9
Mt Isa Supergroup Australia	Eriksson et al. (1992)	1675 ± 30	12	70.6	9.8
Rinconada Group New Mexico, USA	McLennan et al. (1995)	1700 ± 35	12	79.4	3.8
Uncompahgre Group Colorado, USA	McLennan et al. (1995)	1670 ± 40	3	79.8	2.4
Nama Group South Africa	Laskowski and Kroner (1985)	650 ± 40	5	79.7	5.0
Maverick Shale	Condie et al. (1992)	1710 ± 10	15	79.5	7.8

Geologic unit	Reference	Age (Ma)	Number of samples	CIA (Mean)	CIA (std dev)
Arizona, USA	Cox et al. (1995)				
Shaler Supergroup NW Territories, Canada	Young (1981);	1000 ± 70	6	81.6	5.7
Houdan/Flying W Formations Arizona, USA	Condie et al. (1992)	1690 ± 10	10	72.9	3.7
Gorge Creek Group Pilbara, W Australia	McLennan et al. (1983)	3400 ± 15	9	80.0	2.7
Namaqua South Africa	Moore (1989)	1700 ± 25	2	76.8	2.1
Fortesque Group Western Australia	B. Krapez, 1998 Krapez (1999)	2750 ± 20	5	88.7	5.6
San Andres sediments New Mexico, USA	Alford (1987)	1670 ± 20	4	70.9	6.0
Earaheedy Group Western Australia	B. Krapez, 1998 Krapez and Martin (1999)	1700 ± 22	3	83.8	4.2
Pertataka Group Australia	Taylor and McLennan (1985)	850 ± 50	4	78.8	3.2
Kaleva 1 Finland	Kohonen (1995)	2100 ± 100	5	69.4	2.6
Libby Creek Group Wyoming, USA	Crichton and Condie (1993)	2100 ± 50	13	72.0	5.0
Whim Creek Group Western Australia	McLennan et al. (1983)	2700 ± 20	14	87.0	6.5
Namoona Group Northern Australia	Stewart Needham, 1998	2100 ± 120	20	73.6	4.4
Mt Partridge Group Northern Australia	Stewart Needham, 1998	2100 ± 120	28	74.2	2.9
South Alligator Group Northern Australia	Stewart Needham, 1998	1900 ± 100	18	73.0	5.6

Geologic unit	Reference	Age (Ma)	Number of samples	CIA (Mean)	CIA (std dev)
Chocolay Group Minnesota	Nance (1953)	2000 ± 100	4	75.4	1.0
Animike Group Minnesota	Richard Ojakangas, 1998 Nance (1953)	1878 ± 20	10	74.7	3.0
Menominee Group Minnesota	Nance (1953)	1900 ± 20	4	80.2	5.3
Belt Supergroup (Newland Fm) Montana	Schieber (1992)	1450 ± 10	10	71.8	5.0
Grand Canyon Supergroup Arizona, USA	Cox et al. (1995)	1100 ± 60	15	67.4	6.2
Upper Huronian Supergroup Southern Canada	McLennan et al. (1979)	2350 ± 100	5	68.0	1.5
Lower Huronian Supergroup Southern Canada	McLennan et al. (1979)	2350 ± 100	5	75.9	2.3
Epworth Group Northern Canada	Hoffman (1973) K. C. Condie (1998) unpub. Data	1887 ± 35	6	87.2	4.8

Appendix C. Appendix references

Alford, D.E., 1987. Geology and geochemistry of the Hembrillo Canyon succession, San Andres Mountains, Sierra and Dona Ana Counties, NM. Masters thesis, New Mexico Institute of Mining and Technology, Socorro, NM, p. 180.

Altermann, W., Siegfried, H.P., 1994. Sedimentology and facies development of an Archean shelf: carbonate platform transition in the Kaapvaal craton, as deduced from a deep borehole at Kathu, South Africa. J. Afr. Earth Sci. 24, 391–410.

Arndt, N.T., Nelson, D.R., Compston, W., Trendall, A.F., Thorne, A.M., 1991. The age of the Fortescue Group, Hamersley basin, Western Australia, from ion microprobe zircon U/Pb results. Aust. J. Earth Sci. 38, 261–281.

Aspler, L.B., Chiarenzelli, J.R., 1997. Initiation of 2.45–2.1 Ga intracratonic basin sedimentation of the Hurwitz Group, Keewatin hinterland, NW Territories, Canada. Precamb. Res. 81, 265–297.

Barley, M.E., Pickard, A.L., Sylvester, P.J., 1997. Emplacement of a large igneous province as a possible cause of banded iron formation 2.45 Ga. Nature 385, 55–58.

Blake, D.H., Stewart, A.J., 1992. Stratigraphic and tectonic framework, Mount Isa Inlier. Aust. Bur. Min. Res. Bull. 243.

Bose, P.K., Mazumder, R., Sarkar, S., 1997. Tidal sandwaves and related storm deposits in the transgressive Protoproteozoic Chaibasa Formation, India. Precamb. Res. 84, 63–81.

Bennett, G., Dressler, B.O., Robertson, J.A., 1991. The Huronian Supergroup and associated intrusive rocks. Ontario Geol. Survey 4, 549–591.

Condie, K.C., Budding, A.J., 1979. Geology and geochemistry of Precambrian rocks, central and southcentral New Mexico, New Mexico Bureau of Mines and Mineral Resources, Memoir 35, p. 58

Condie, K.C., Noll, Jr., P.D., Conway, C.M., 1992. Geochemical and detrital mode evidence for two sources of Early Proterozoic sedimentary rocks from the Tonto Basin Supergroup, Central Arizona. Sedimentary Geology 77, 51–76.

Condie, K.C., Dengate, J., Cullers, R.L., 1995. Behavior of rare earth elements in a paleoweathering profile on granodiorite in the Front Range, Colorado Geochim. Cosmochim. Acta 59, 279–294.

Cox, R., Lowe, D.R., Cullers, R.L., 1995. The influence of sediment recycling and basement composition on evolution of mudrock chemistry in the southwestern United States. Geochim. Cosmochim. Acta 59, 2919–2940.

Crichton, J.G., 1992. Geochemistry and provenance of the Early Proterozoic Libby Creek Group, Medicine Bow Mountains, Southeastern Wyoming. Masters thesis, New Mexico Institute of Mining Technology, Socorro, NM, p. 95.

Crichton, J.G., Condie, K.C., 1993. Trace elements as source indicators in cratonic sediments:

A case study from the Early Proterozoic Libby Creek Group, Southeastern Wyoming. J. Geol. 101, 319–332.
Donnelly, T.H., Crick, I.H., 1988. Depositional environment of the Middle Proterozoic Velkerri Formation in Northern Australia: geochemical evidence. Precamb. Res. 42, 165–172.
Eisbacher, G.H., 1985. Late Proterozoic rifting, glacial sedimentation, and sedimentary cycles in the light of Windermere deposition, Western Canada. Paleogeo. Paleoclimat. Paleoecology, 51, 231–254.
Eriksson, K.A., Taylor, S.R., Korsch, R.J., 1992. Geochemistry of 1.8–1.67 Ga mudstones and siltstones from the Mount Isa Inlier, Queensland, Australia: provenance and tectonic implications. Geochim. Cosmochim. Acta 56, 899–909.
Eriksson, P.G. et al., 1994. Early Proterozoic black shales of the Timeball Hill Formation, South Africa: volcanogenic and paleoenvironmental influences. J. Afr. Earth Sci. 18, 325–337.
Ewers, G.R., Higgins, N.C., 1985. Geochemistry of the Early Proterozoic metasedimentary rocks of the Alligator Rivers region, Northern Territory, Australia. Precamb. Res. 29, 331–357.
Ewers, G.R., Needham, R.S., Stuart-Smith, P.G., Crick, I.H., 1985. Geochemistry of the low-grade Early Proterozoic sedimentary sequence in the Pine Creek geosyncline, Northern Territory. Aust. J. Earth Sci. 32, 137–154.
Fedo, C.M., Young, G.M., Nesbitt, H.W., 1997. Paleoclimatic control on composition of the Paleoproterozoic Serpent Formation, Huronian Supergroup, Canada: a greenhouse to icehouse transition. Precamb. Res. 86, 201–223.
Fedo, C.M., Eriksson, K.A., Krogstad, E.J., 1996. Geochemistry of shales from the Archean Buhwa greenstone belt, Zimbabwe: implications for provenance and source-area weathering. Geochim. Cosmochim. Acta 60, 1751–1763.
Gabrielse, H., Yorath, C.J., 1992. Geology of the Cordilleran orogen in Canada. Geol. Soc. America, Decade of North American Geology, v. G-2.
Gibbs, A.K., Barron, C.N., 1993. The geology of the Guiana shield. Oxford University Press, NY.
Gibbs, A.K., Montgomery, C.W., O'Day, P.A., Erslev, E.A., 1986. The Archean–Proterozoic transition: evidence from the geochemistry of metasedimentary rocks of Guyana and Montana. Geochim. Cosmochim. Acta 50, 2125–2141.
Hayashi, K., Fujisawa, H., Holland, H.D., Ohmoto, H., 1997. Geochemistry of 1.9 Ga sedimentary rocks from NE Labrador, Canada. Geochim. Cosmochim. Acta 61, 4115–4137.
Heaman, L.M., LeCheminant, A.N., 1993. Paragenesis and U/Pb systematics of baddeleyite. Chem. Geol. 110, 95–126.
Hoffman, P., 1973. Evolution of an Early Proterozoic continental margin: the Coronation geosyncline and associated aulacogens of the NW Canadian shield. Phil. Trans. R. Soc. Lond. 273A, 547–581.
Jackson, G.D., Iannelli, T.R., Narbonne, G.M., Wallace, P.J., 1978. Upper Proterozoic sedimentary and volcanic rocks of NW Baffin Island. Geol. Surv. Can., paper 78–14.
Jackson, M.J., Raiswell, R., 1991. Sedimentology and carbon–sulphur geochemistry of the Velkerri Formation, a Mid-Proterozoic potential oil source in northern Australia. Precamb. Res. 54, 81–108.
Kale, V.S., Phansalkar, V.G., 1991. Purana basins of peninsular India: a review. Basin Res. 3, 1–36.
Karlstrom, K.E., Flurkey, A.J., Houston, R.S., 1983. Stratigraphy and depositional setting of the Proterozoic Snowy Pass Supergroup, SE Wyoming: record of an Early Proterozoic Atlantic-type cratonic margin. Geol. Soc. Am. Bull. 94, 1257–1274.
Kohonen, J., 1995. From continental rifting to collisional crustal shortening-Paleoproterozoic Kaleva metasediments of the Hoytiainen area in N. Karelia, Finland. Geol. Surv. Finland, Bull. 380, p. 79.
Krapez, B., 1999. Stratigraphic record of an Atlantic-type global tectonic cycle in the Paleoproterozoic Ashburton Province of Western Australia. Aust. J. Earth Sci. 46, 71–87.
Krapez, B., Martin, McB., 1999. Contrasting sequence-stratigraphic records of the southern Andean-type marginal basin and a strike-slip basin in the Paleoproterozoic Nabberu Province of Western Australia. Aust. J. Earth Sci. 46, 89–103.
Laskowski, N., Kroner, A., 1985. Geochemical characteristics of Archean and Late Proterozoic to Paleozoic fine-grained sediments from southern Africa and significance for the evolution of the continental crust. Geol. Rund. 74/1, 1–9.
Leblanc, M., Moussine-Pouchkine, A., 1994. Sedimentary and volcanic evolution of a Neoproterozoic continental margin (Bleida, Anti-Atlas, Morocco). Precamb. Res. 70, 25–44.
Link, P.K. et al., 1993. Middle and Late Proterozoic stratified rocks of the western US Cordillera, Colorado Plateau, and Basin and Range Province. Geol. Soc. Am., Geology of North America, C-2, 463–596.
Litherland, M. et al., 1986. The geology and mineral resources of the Bolivian Precambrian shield. Br. Geol. Surv., Overseas Mem. 9.
Maas, R., McCulloch, M.T., 1991. The provenance of Archean clastic metasediments in the Narryer gneiss complex, Western Australia: trace element geochemistry, Nd isotopes, and U/Pb ages for detrital zircons. Geochim. Cosmochim. Acta 55, 1915–1932.
Mansey, J.L., Gabrielse, H., 1978. Stratigraphy, terminology and correlation of upper Proterozoic rocks in Omineca and Cassiar Mountains, north-central British Columbia. Geol. Surv. Canada, paper 77–19, p. 17.
Master, S., 1991. Stratigraphy, tectonic setting, and mineralization of the Early Proterozoic Magondi Supergroup, Zimbabwe: a review. Econ. Geol. Res. Unit, Info. Circ. 238, p. 75.
Matthai, S.K., Henley, R.W., 1996. Geochemistry and depositional environment of the gold-mineralized Proterozoic Koolpin Formation, Pine Creek Inlier, Northern Australia: a comparison with modern shale sequences. Precamb. Res. 78, 211–235.
McLennan, S.M., Taylor, S.R., Eriksson, K.A., 1983. Geochemistry of Archean shales from the Pilbara Supergroup, Western Australia. Geochim. Cosmochim. Acta 47, 1211–1222.
McLennan, S.M., Taylor, S.R., Kroner, A., 1983. Geochemical evolution of Archean shales from South Africa 1. The Swaziland and Pongola Supergroups. Precamb. Res. 22, 93–124.
Moore, J.M., 1989. A comparative study of metamorphosed supracrustal rocks from the western Namaqualand metamorphic complex. Precamb. Res. Unit, University of Cape Town, Bull. 37.

Nance, Jr., R.H., 1953. Chemical composition of Precambrian slates with notes on the geochemical evolution of lutites. J. Geol. 61, 51–64.
Needham, R.S., Stuart-Smith, P.G., Page, R.W., 1988. Tectonic evolution of the Pine Creek inlier, Northern Territory. Precamb. Res. 40/41, 543–564.
Rainbird, R.H., Jefferson, C.W., Young, G.M., 1996. The early Neoproterozoic sedimentary succession B of NW Laurentia: correlations and paleogeographic significance. Geol. Soc. Am. Bull. 108, 454–470.
Rainbird, R.H., 1991. Stratigraphy, sedimentology and tectonic setting of the upper Shaler Group, Victoria Island, NW Territories. PhD dissertation, University of Western Ontario, London, Ontario, p. 257.
Rao, V.V.S., Sreenivas, B., Balaram, V., Bovil, P.K., Srinivasan, R., 1999. Nature of Archean upper crust as revealed from the geochemistry of Proterozoic shales of the Kaladgi basin, Karnataka, southern India. Precamb. Res. 98, 53–65.
Ricketts, B.D., Donaldson, J.A., 1981. Sedimentary history of the Belcher Group of Hudson Bay. Geol. Surv. Canada, paper 81–10, 235–254.
Roberts, M.T., 1974. Stratigraphy and depositional environments of the Crystal Spring Formation, Southern Death Valley region, California. Geol. Soc. Am., Guidebook to Death Valley Region, California and Nevada.
Schieber, J., 1992. A combined petrographical–geochemical provenance study of the Newland Formation, Mid-Proterozoic of Montana. Geol. Mag. 129, 223–237.
Soegaard, K., Eriksson, K.A., 1985. Evidence of tide, storm, and wave interaction on a Precambrian siliciclastic shelf: the 1700 My Ortega Group, New Mexico. J. Sed. Petrol. 55, 672–684.
Taylor, S.R., McLennan, S.M., 1983. Geochemistry of Early Proterozoic sedimentary rocks and the Archean/Proterozoic boundary. Geol. Soc. Am. Mem. 161, 119–129.
Taylor S.R., McLennan, S.M.,1985. The Continental Crust: Its Composition and Evolution: Blackwell, Oxford, p. 312.
Ugidos, J.M., Valladares, M.I., Recio, C., Rogers, G., Fallick, A.E., Stephens, W.E., 1997. Provenance of upper Precambrian–lower Cambrian shales in the central Iberian zone, Spain: evidence from a chemical and isotopic study. Chem. Geol. 136, 55–70.
Ugidos, J.M., Armenteros, I., Barba, P., Valladares, M.I., Colmenero, J.R., 1997. Geochemistry and petrology, recycled orogen sediments: Late Proterozoic, siliclastic rocks, Central Iberian zone, Spain. Precamb. Res. 84, 163–180.
Willis, I.L., Brown, R.E., Stroud, W.J., Stevens, B.P.J., 1983. The Early Proterozoic Willyama Supergroup: stratigraphic subdivision and interpretation of high to low-grade metamorphic rocks in the Broken Hill block, New South Wales. J. Geol. Soc. Aust. 30, 195–224.
Winston, D., 1990. Evidence for intracratonic, fluvial and lacustrin settings of Middle to Late Proterozoic basins of Western USA. Geol. Assoc. Canada, Spec. Paper 38, 535–564.
Wronkiewicz, D.J., Condie, K.C., 1987. Geochemistry of Archean shales from the Witwatersrand Supergroup, South Africa: Source-area weathering and provenance. Geochim. Cosmochim. Acta 51, 2401–2416.
Wronkiewicz, D.J., Condie, K.C., 1989. Geochemistry and provenance of sediments from the Pongola Supergroup South Africa: evidence for a 3.0-Ga-old continental craton. Geochim. Cosmochim. Acta 53, 1537–1549.
Wronkiewicz, D.J., Condie, K.C., 1990. Geochemistry and mineralogy of sediments from the Ventersdorp and Transvaal Supergroups, South Africa: Cratonic evolution during the early Proterozoic. Geochim. Cosmochim. Acta 54, 343–354.
Young, G.M., 1981. The Amundsen embayment, N.W.T.: relevance to the upper Proterozoic evolution of North America. In: Campbell, F.H.A. (Ed.), Geol. Surv. Canada, paper 81–10, pp. 203–218.

References

Berner, R.A., 1983. Burial of organic carbon and pyrite sulfur in sediments over Phanerozoic time: a new theory. Geochim. Cosmochim. Acta 47, 855–862.
Berner, R.A., Berner, E.K., 1997. Silicate weathering and climate. In: Ruddiman, W.F. (Ed.), Tectonic uplift and climate change, Plenum Press, New York.
Berry, W.B.N., Wilde, P., 1978. Progressive ventilation of the oceans — an explanation for the distribution of the lower Paleozoic black shales. Am. Jour Sci. 278, 257–275.
Betts, J.N., Holland, H.D., 1991. The oxygen content of ocean bottom waters, the burial efficiency of organic carbon, and the regulation of atmospheric oxygen. Palaeogeogr. Palaeoclimatol. Palaeoecol. 97, 5–18.
Beukes, J.J., Klein, C., Kaufman, A.J., Hayes, J.M., 1990. Carbonate petrography, kerogen distribution, and carbon and oxygen isotope variations in an early Proterozoic transition from limestone to iron-formation deposition, Transvaal Supergroup, South Africa. Bull. Soc. Econ. Geol. 85, 663–690.
Bickle, M.J., 1996. Metamorphic decarbonation, silicate weathering and the long-term carbon cycle. Terra Nova 8, 270–276.
Caldeira, K., Rampino, M.R., 1991. The mid-Cretaceous superplume, carbon dioxide, and global warming. Geophys. Res. Lett. 18, 987–990.
Canfield, D.E., 1998. A new model for Proterozoic ocean chemistry. Nature 396, 450–453.
Condie, K.C., 1993. Chemical composition and evolution of the upper continental crust: contrasting results from surface samples and shales. Chem. Geol. 104, 1–37.
Condie, K.C., 1998. Episodic continental growth and supercontinents: a mantle avalanche connection? Earth Planet Sci. Lett. 163, 97–108.
Condie, K.C., 2000. Continental Growth During Formation of Rodinia at 1.35–0.9 Ga. Gondwana Res. (in press).
Derry, L.A., Kaufman, A.J., Jacobsen, S.B., 1992. Sedimentary cycling and environmental change in the Late Proterozoic: evidence from stable and radiogenic isotopes. Geochim. Cosmochim. Acta 56, 1317–1329.

Des Marais, D.J., Moore, J.G., 1984. Carbon and its isotopes in mid-oceanic basaltic glasses. Earth Planet Sci. Lett. 69, 43–57.

Des Marais, D.J., Strauss, H., Summons, R.E., Hayes, J.M., 1992. Carbon isotope evidence for the stepwise oxidation of the Proterozoic environment. Nature 359, 605–609.

Des Marais, D.J., 1997. Long-term evolution of the biogeochemical carbon cycle. In: Banfield, J., Nealson, K. (Eds.), Geomicrobiology. Mineralog. Association of America, Washington DC, pp. 429–445.

Greff-Lefftz, M., Legros, H., 1999. Core rotational dynamics and geological events. Science 286, 1707–1709.

Grotzinger, J.P., Kasting, J.F., 1993. New constraints on Precambrian ocean composition. J. Geol. 101, 235–243.

Haaq, B.U., 1998. Gas hydrates: greenhouse nightmare? Energy panacea or pipe dream? GSA Today 8 (11), 1–6.

Hofmann, H.J., 1998. Synopsis of Precambrian fossil occurrences in North America. Geol. Soc. America, Decade of North American Geology, v. C-1: 273–293.

Holland, H.D., 1984. The Chemical Evolution of the Atmosphere and Oceans. Princeton University Press, Princeton, New Jersey.

Holser, W.T., Schidlowski, M., Mackenzie, F.T., Maynard, J.B., 1988. Geochemical cycles of carbon and sulfur. In: Gregor, C.B., Garrels, R.M., Mackenzie, F.T., Maynard, J.B. (Eds.), Chemical Cycles in the Evolution of the Earth. Wiley, New York, pp. 105–173.

Isley, A.E., Abbott, D.H., 1999. Plume-related mafic volcanism and the deposition of banded iron formation. J. Geophys. Res. 104, 15461–15477.

Jyotiranjan, S.R., Ramesh, R., Pande, K., 1999. Carbon isotopes in Kerguelen plume-derived carbonalities: evidence for recycled inorganic carbon. Earth Planet Sci. Lett. 170, 205–214.

Karhu, J.A., Holland, H.D., 1996. Carbon isotopes and the rise of atmospheric oxygen. Geology 24, 867–870.

Kaufman, A.J., 1997. An ice age in the tropics. Nature 386, 227–228.

Kerr, A.C., 1998. Oceanic plateau formation: a cause of mass extinction and black shale deposition around the Cenomanian–Turonian boundary? J. Geol. Soc. Lond. 155, 619–626.

Knoll, A.H., Canfield, D.E., 1998. Isotopic inferences on early ecosystems. Paleontol. Soc. Papers 4, 212–243.

Larson, R.L., 1991a. Latest pulse of Earth: evidence for a mid-Cretaceous superplume. Geology 19, 547–550.

Larson, R.L., 1991b. Geological consequences of superplumes. Geology 19, 963–966.

Melezhik, V.A., Fallick, A.E., 1996. A widespread positive $\delta^{13}C$ anomaly at around 2.33–2.06 Ga on the Fennoscandian shield: a paradox? Terra Nova 8, 141–157.

Nesbitt, H.W., Young, G.M., 1982. Early Proterozoic climates and plate motions inferred from major element chemistry of lutites. Nature 299, 715–717.

Nesbitt, H.W., Young, G.M., McLennan, S.M., Keays, R.R., 1996. Effects of chemical weathering and sorting on the petrogenesis fo siliciclastic sediment, with implications for provenance studies. J. Geol. 104, 525–542.

Rogers, J.J.W., 1996. A history of continents in the past three billion years. J. Geol. 104, 91–107.

Taylor, S.R., McLennan, S.M., 1985. The Continental Crust: Its Composition and Evolution. Blackwell, London, p. 312.

Veizer, J., 1988. The evolving exogenic cycle. In: Gregor, C.B., Garrels, R.M., Mackenzie, F.T., Maynard, J.B. (Eds.), Chemical Cycles in the Evolution of the Earth. Wiley, New York, pp. 175–219.

Worsley, T.R., Nance, R.D., Moody, J.B., 1986. Tectonic cycles and the history of the earth's biogeochemical and paleoceanographic record. Paleoceanography 1, 233–263.

Worsley, T.R., Nance, R.D., 1989. Carbon redox and climate control through earth history: a speculative reconstruction. Palaeogeog. Palaeoclimat. Palaeoecol. 75, 259–282.

Young, G.M., 1991. The geologic record of glaciation: relevance to the climatic history of Earth. Geosci. Can. 100–108, 18.